frontiers | Frontiers in Astronomy and Space Sciences

TYPE Original Research
PUBLISHED 19 December 2024
DOI 10.3389/fspas.2024.1520141

OPEN ACCESS

EDITED BY
Boyi Wang,
Harbin Institute of Technology, China

REVIEWED BY
Alexei V. Dmitriev,
Lomonosov Moscow State University, Russia
Kun Zhang,
University of California, Los Angeles, United States

*CORRESPONDENCE
Xingran Chen,
chenxingran@must.edu.mo

RECEIVED 30 October 2024
ACCEPTED 20 November 2024
PUBLISHED 19 December 2024

CITATION
Chen X, Lu X, Zong Q, Zhang H, Liu Y and Zhou X (2024) Shock-induced radiation belt dynamics: simultaneous observations of "one-kick" acceleration and ultralow frequency modulation.
Front. Astron. Space Sci. 11:1520141.
doi: 10.3389/fspas.2024.1520141

Shock-induced radiation belt dynamics: simultaneous observations of "one-kick" acceleration and ultralow frequency modulation

Xingran Chen[1,2]*, Xi Lu[3,2], Qiugang Zong[1,4], Hui Zhang[5,2], Ying Liu[1] and Xuzhi Zhou[4]

[1]State Key Laboratory of Lunar and Planetary Science, Macau University of Science and Technology, Macau SAR, China, [2]Geophysical Institute, University of Alaska Fairbanks, Fairbanks, AK, United States, [3]William B. Hanson Center for Space Sciences, University of Taxes at Dallas, Richardson, TX, United States, [4]Institute of Space Physics and Applied Technology, Peking University, Beijing, China, [5]School of Space Science and Technology, Shandong University, Weihai, China

We present conjunctive observations to study the prompt responses of radiation belt electrons during the interplanetary shock (IPS) event on 7 September 2017. As the IPS impinged the Earth, the Time History of Events and Macroscale Interactions (THEMIS) E spacecraft located near the dayside bow shock observed alternating features of solar wind and magnetosheath, indicating that the magnetosphere was repeatedly compressed. Following each compression, rapid increases of relativistic electron fluxes and the corresponding drift echoes were well identified over the energy and pitch-angle spectra obtained by the Van Allen Probes (RBSP) in the inner magnetosphere. Meanwhile, oscillations in the Pc4 range are embedded in the flux variations, appearing as straight stripes in the pitch-angle distributions observed by RBSP-B inside the wave active region and "boomerang" stripes in the observations obtained by RBSP-A ~6 MLT away. Such diverse signatures suggested an azimuthally confined ultralow frequency (ULF) wave. The patterns in the observed particle spectra agreed well with the theoretical predictions, by which we conclude that the surfing acceleration by the shock-induced pulse and the continuous modulation by the localized ULF wave conspired to cause significant disturbances to the Earth's radiation belt.

KEYWORDS

radiation belt, energetic electron, interplanetary shock, surfing acceleration, ultralow frequency wave, space weather

1 Introduction

The dynamics of radiation belt electrons is an outstanding yet unresolved question of geophysics (Friedel et al., 2002; Ripoll et al., 2020). Sudden increases of energetic electron flux in the inner magnetosphere can put space activities at risk, since astronauts and electronic devices are vulnerable under the exposure to these "killer" electrons (Zong et al., 2009). A number of fast relativistic electron buildup events were found to be correlated with the impact of an interplanetary shock (IPS) (Wilken et al., 1982; Blake et al., 1992; Foster et al., 2015; Kanekal et al., 2016; Hao et al., 2019; Zhang et al., 2024). The most well-known example of such shock-induced

radiation belt enhancement was recorded by the Combined Release and Radiation Effects Satellite (CRRES) during the intense storm sudden commencement (SSC) on 24 March 1991. Injection of ultra-relativistic (~15 MeV) electrons deep into the former slot region ($L \sim 2.5$) and large-amplitude (~40 mV/m) bipolar electric field impulse were observed almost instantaneously by the IPS arrival (Blake et al., 1992; Wygant et al., 1994). These unprecedented observations were first simulated by Li et al. (1993) using a guiding center test particle code. The impulsive electric field (IEF) swept through the radiation belt at a speed comparable to the drift velocity (in the order of 10^3 km/s) of the ultra-relativistic electrons. Those electrons in resonance with the pulse would be substantially accelerated and inward transported within a fraction of their drift period, which in turn can explain the prompt electron flux enhancement observed by CRRES. This model of radiation belt dynamics in response to IPS impingement is commonly referred to as the "one-kick" scenario, noting that the particles are efficiently energized mainly during the single passage of the shock-induced pulse. The physical framework has been complemented by magnetohydrodynamics (MHD) simulations (Hudson et al., 1997; Elkington et al., 2002) and successfully applied to several other events (Kanekal et al., 2016; Schiller et al., 2016; Hudson et al., 2017). In all these events, the initial flux enhancements of the relativistic electrons at different energies were followed by recurrent echoes at their respective drift periods. This periodic feature, known as the "drift echoes", is consistent with the theoretical prediction of the one-kick mechanism and widely used as a characteristic signature to understand the particle dynamics in the radiation belt (Hudson et al., 2020). However, Zong et al. (2009) reported coherent oscillations, distinct from the drift echoes, in the cases of both strong and weak IPS. The quasi-monochromatic ultralow frequency (ULF) oscillations were identified in the electromagnetic fields and across the energetic electron spectra. These ULF wave signatures were further attributed to the drift-resonance interaction (Southwood and Kivelson, 1981) between the magnetospheric electrons and the transverse Alfven waves excited by the IPS impingement. Subsequent studies also confirmed the important role of ULF waves in the shock-induced radiation belt dynamics (Zong et al., 2012; Mann et al., 2013; Hao et al., 2014; Foster et al., 2015; Zhang et al., 2020).

Although the significance of IEF and ULF wave has been generally acknowledged, the debate goes on about the dominant factor controlling the shock-induced radiation belt dynamics. A recent ultra-relativistic electron enhancement event, triggered by the IPS impingement on 16 July 2017, was studied by Hao et al. (2019) and Patel et al. (2019), in which the same observational data were analyzed but different physical pictures were suggested. Hao et al. (2019) verified the resonance condition and ascribed the electron flux variation observed by the Van Allen Probes to the drift-resonance interaction with the $m = 1$ poloidal mode ULF wave. They also pinpointed the "group-N" stripes in the electron flux spectrogram which could only be recognized away from the resonant energy (< 2 MeV) as circumstantial evidence for the ULF wave-particle interaction scenario. In addition, their conclusion was reinforced by the consistency between the observed particle signatures and the electron energy change calculated numerically on the basis of the revised drift-resonance theory (Zhou et al., 2016). In contrast, Patel et al. (2019) modeled the event via a MHD-test particle simulation where the energization and drift phase bunching of the electrons were driven by the shock-induced pulse. The time series and the energy spectra of the ultra-relativistic (~2 to 6 MeV) electron flux were, to a considerable extent, reproduced. Thus, Patel et al. (2019) argued that the one-kick mechanism alone could explain the electron dynamics in response to the IPS impact. Since both drift echoes and ULF modulations basically appear as periodic patterns, it could be controversial to evaluate the similarity between the actual measurements and the virtual observations, thereby leaving room for ambiguity in interpreting the data.

Nevertheless, the controversy depicts the necessity to outline the characteristic features to discriminate between the one-kick acceleration and the continuous ULF wave-particle interaction. In this paper, we investigate another typical IPS event on 7 September 2017 (Zhang et al., 2024). The signatures of drift echoes and ULF modulations were unambiguously extracted from the *in situ* measurements of radiation belt electrons. Our observations show that the two mechanisms conspired to cause the electron flux variations with comparable contributions.

2 Observations

Multi-point observations by the Advanced Composition Explorer (ACE), the Time History of Events and Macroscale Interactions during Substorms (THEMIS) spacecraft, and the Van Allen Probes (also known as the Radiation Belt Storm Probes, RBSP) are employed to study the IPS event on 7 September 2017. As shown in Figures 1a–c, an interplanetary fast forward shock transited ACE, which was located around the first Lagrangian point, at ~22:35 UT. The shock passage is characterized by an abrupt change of the plasma parameters. The southward interplanetary magnetic field (negative IMF B_z) enhanced from −10 nT to ~-25 nT. The solar wind velocity jumped from ~470 km/s to ~700 km/s and the proton number density doubled, which means that the dynamic pressure multiplied by a factor of ~3. The IPS then struck the Earth at ~23:00 UT, as registered by THEMIS-E in the dayside magnetosheath. The abrupt increase of dynamic pressure resulted in a prompt compression of the magnetosheath, manifested by an instantaneous enhancement of ion energy flux (shown in Figure 1e). It is notable that the energy flux spectrogram suddenly presented as a narrow beam-like structure ~80 s after the shock arrival. In contrast to the thermalized magnetosheath plasma, the ion beam concentrated at ~3 keV (corresponding to ~ 700 km/s), which indicates that the spacecraft crossed the bow shock into the solar wind. In other words, the magnetosphere was highly compressed by the shock-associated pressure pulse, so that THEMIS-E suddenly found itself out of the magnetosheath. Meanwhile, the SYM-H index (shown in Figure 1d) increased by 40 nT within 2 min. The sharp increase of SYM-H index, which is a typical feature of SSC (Chapman and Ferraro, 1940; Dessler et al., 1960), corresponded to the rapidly enhanced magnetopause current caused by the shock impingement. Additionally, we infer from the alternating features of magnetosheath and solar wind observed by THEMIS-E that the bow shock was moving to-and-fro during the event.

Herein, we focus on the initial shock-induced compression at ~23:00 UT and investigate the corresponding magnetospheric

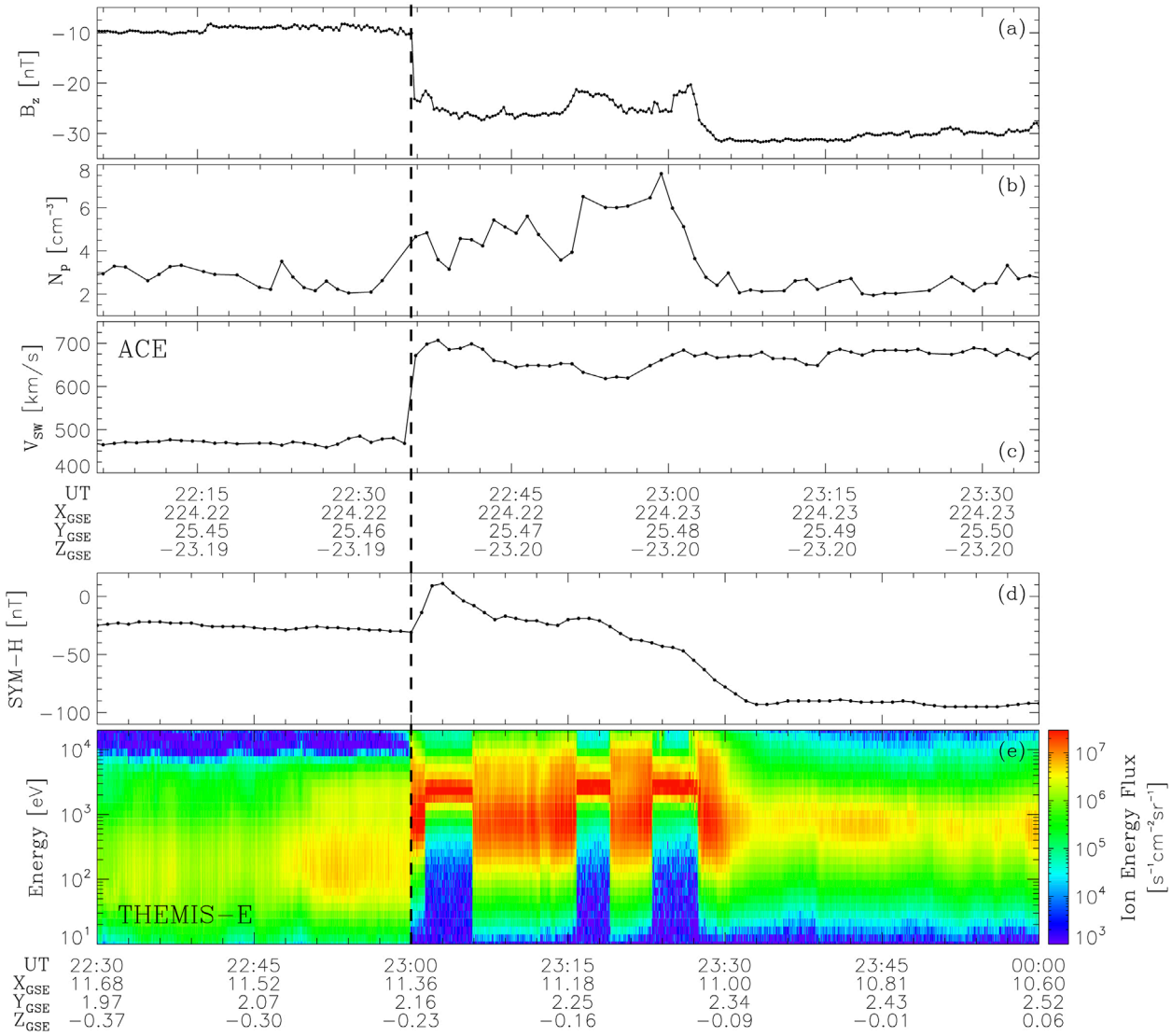

FIGURE 1
Overview of the 7 September 2017 interplanetary shock. **(a)** Z-component of the interplanetary magnetic field B_z, **(b)** proton number density N_p, and **(c)** bulk velocity V_{SW} observed by ACE in the solar wind. **(d)** SYM-H index. **(e)** Energy-time spectrogram of ion energy flux observed by THEMIS-E near the Bow shock. The vertical dashed line (here and in every other figures) marks the shock arrival at the dayside magnetosheath (23:00 UT).

responses. Figure 2 presents the electron differential flux measured by the Magnetic Electron Ion Spectrometer (MagEIS) (Blake et al., 2013) and the Relativistic Electron and Proton Telescope (REPT) (Baker et al., 2013) onboard the twin Van Allen Probes between 22:50 and 23:30 UT. During this interval, RBSP-A traveled inbound through the dusk-side (MLT ~15) outer radiation belt (L from ~5 to ~4) while RBSP-B was on its outbound pass (L from ~3 to ~4) in the dawn (MLT ~9) sector (See Figure 5 for the trajectories of the Van Allen Probes). Both RBSP-A and RBSP-B observed significant flux enhancements within 1 min after the IPS impinged on the dayside magnetosheath. The subsequent recurrences of the enhanced electron fluxes were also recorded by both spacecrafts. In other words, the radiation belt electron fluxes presented periodic variations, similar to previous studies (Zong et al., 2009; Foster et al., 2015; Hao et al., 2019). However, as shown in the pitch angle-time spectrograms, two types of periodic patterns can be recognized by their distinct periods. Specifically, recurrent echoes corresponding to the drift periods of the relativistic electrons, in the order of 10^3 *s*, were readily apparent. These periodic variations, identified as drift echoes, was attributed to the surfing acceleration by the shock-induced IEF (Zhang et al., 2024). Besides, the electron fluxes were observed to oscillate at the period of ~90 *s*. These Pc4 (Jacobs et al., 1964) oscillations appeared as dispersionless straight stripes in the observations of RBSP-B (Figures 2c–n, right panels). The stripes occurred almost immediately after the shock arrival and persisted for several cycles. The ~90 *s* oscillations were also presented in the observations of RBSP-A in the form of boomerang stripes (Hao et al., 2017). The oscillating boomerang-shaped patterns were most obvious at the 470, 597, and 749 *keV* energy channels (Figures 2C–E). As for higher energies, the patterns

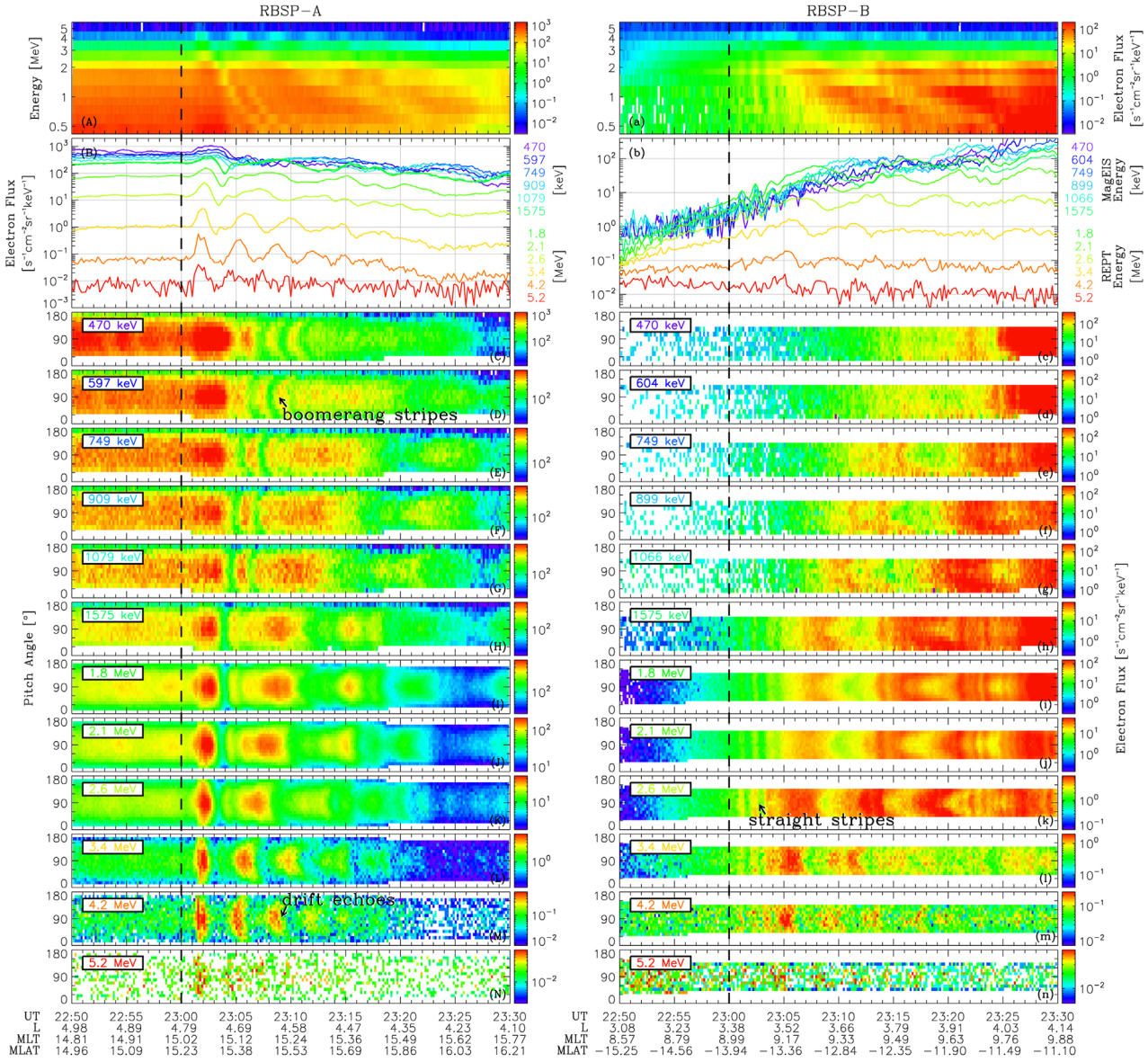

FIGURE 2
Observations of radiation belt electrons. **(A)** Energy-time spectrogram and **(B)** time series plot of electron fluxes measured by Van Allen Probe A. **(C–N)** Electron pitch angle distribution obtained by Van Allen Probe A. **(a–n)** Van Allen Probe B observations in the same format as Panels A–N. Typical patterns of the electron flux spectrum are annotated in Panels D, M, and k.

could still be recognized though they were embedded in the drift echoes. The correlation between the different-shaped stripes will be analyzed in Section 3. We will further demonstrate that the straight and boomerang stripes are the manifestations of localized ULF wave-particle interaction inside and outside the wave active region respectively. We will also apply wavelet analysis to achieve a more quantitative description of the electron flux variations.

Before elaborating on the particle signatures, we present the accompanied observations of electromagnetic fields. The magnetic fields measured by the Electric and Magnetic Field Instrument Suite and Integrated Science (EMFISIS) (Kletzing et al., 2013) onboard the Van Allen Probes are shown in Figures 3A–D and 3a–3d. Note that the International Geomagnetic Reference Field (IGRF) is subtracted. Thus, the background magnetic field associated with the change of spacecraft position is removed. In other words, the remaining variations represent the perturbations of the geomagnetic field caused by the IPS impingement. Here, we focus on the observations between 23:00 and 23:10 UT (highlighted with gray shades in Figure 3), since the instant response to the initial shock-induced compression is of our primary interest. As shown in Figures 3b, c, quasi-monochromatic ULF waves were observed by RBSP-B in the morning-side magnetosphere. The dominant period of the wave was ~90 *s*, the same as the stripes in the particle observations. In contrast, RBSP-A, located in the afternoon side (shown in Figures 3A–D), mainly recorded a rapid change of magnetic field (tens of *nT* within 2 min) whereas the coherent

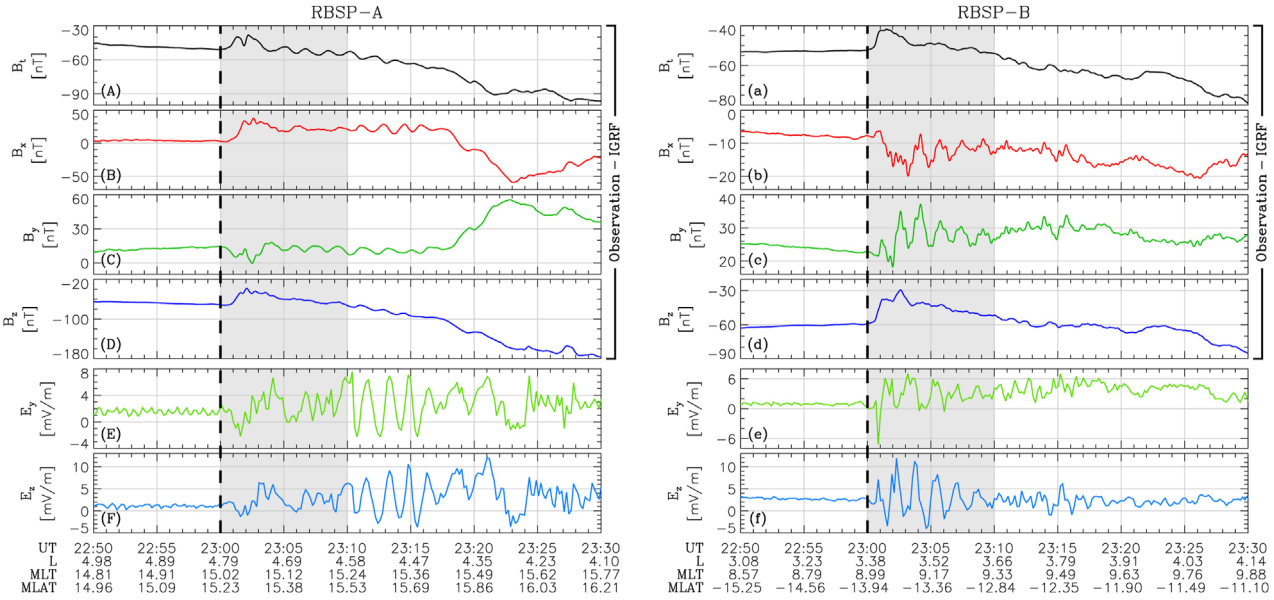

FIGURE 3
In-situ measurements of electric and magnetic fields. Van Allen Probe A observations of **(A)** magnetic field magnitude, **(B–D)** x,y, and z components of the magnetic field vector in the geocentric solar elliptic (GSE) coordinates, **(E, F)** y and z components of the electric field in the modified-GSE coordinates. **(a–f)** Van Allen Probe B observations in the same format as Panels A–F. The magnetic field measurements are presented with the International Geomagnetic Reference Field (IGRF) subtracted. The gray shades highlight the first 10 minutes following the shock arrival.

ULF signals were less apparent (see Supplementary Figure S1 in the supplementary materials for a more quantitative description of the wave amplitude). The local time dependent feature also occurred in the electric field measurements obtained by the Electric Field and Waves (EFW) instrument (Wygant et al., 2013). As shown in Figures 3E, F and 3e, 3f, for the first 10 minutes after the shock arrival, continuous ULF oscillations were only observed by RBSP-B at MLT ~9, while the electric field measured by RBSP-A at MLT ~15 appeared as irregular pulsations. Additionally, it is notable that large amplitude coherent ULF oscillations were also detected by RBSP-A later on (from ~23:10 to ~23:15 UT, Figures 3E, F). Besides, the magnetic field magnitude measured by RBSP-A exhibited periodic fluctuations (from ~23:05 to ~23:15 UT, Figure 3A), which might be associated with a compressional wave. We present a short discussion of these features in the Supplementary Material and leave them for future studies. In brief, the coordinated observations of electric and magnetic fields indicated that the transverse ULF wave immediately following the IPS arrival was localized in the dawn-side magnetosphere.

3 Interpretations and discussions

In contrast to previous studies where the one-kick acceleration by the shock-induced pulse and the continuous interaction with the ULF waves were regarded as competing scenarios, the co-existence of the two different types of periodic electron flux variations described in Section 2 implies that the two mechanisms applied a combined effect to the Earth's radiation belt. The characteristic particle signatures in the present event are highlighted in Figure 4, in the form of electron residual flux. The residual flux is defined as $\frac{j-j_0}{j_0}$, where j is the flux observed in a given energy channel and j_0 is the running average of j. Since the long-term trend is subtracted, the short-term perturbations upon the shock arrival are more explicitly visualized by the residual fluxes. The dispersion characteristics of the two types of periodic signatures can be clearly distinguished in Figures 4A, a. The patterns of drift echoes are increasingly tilted while the patterns of ULF waves are basically parallel. Additionally, as shown in Figures 4B, D, the boomerang stripes of ~ 90 *s* cadence can now be unambiguously identified in the MeV energy channels around 23:04 UT (whereas the shape of the corresponding stripes is less obvious in Figures 2I, K). Thus, Figure 4 strengthens our arguments on the electron flux observations that the multiple periodic features result from the combined effect of the one-kick acceleration and the ULF wave-particle interaction.

To substantiate our interpretations of the observational data, we quantitatively analyze the timing of the periodic patterns in the particle signatures. In general terms, provided a single increase of electron flux occurring over a limited azimuthal range around the magnetic local time ϕ^* at the time t^*, a particle detector located at ϕ might record a sequence of flux enhancements, as the electrons would move periodically along their drift shell. The timing of the n-th observation of the increased flux t_n is given by:

$$\frac{t_n - t^*}{T_d} = \frac{\phi - \phi^*}{24} + n - n_0 \tag{1}$$

where n_0 equals to 0 if $\phi < \phi^*$, otherwise n_0 equals to 1. The electron drift period T_d can be approximated by (Hamlin et al., 1961):

$$T_d = \frac{\pi |e| B_E R_E^2}{3\gamma m_e v^2 L}\left(0.35 + 0.15 \sin \alpha_{eq}\right)^{-1} \tag{2}$$

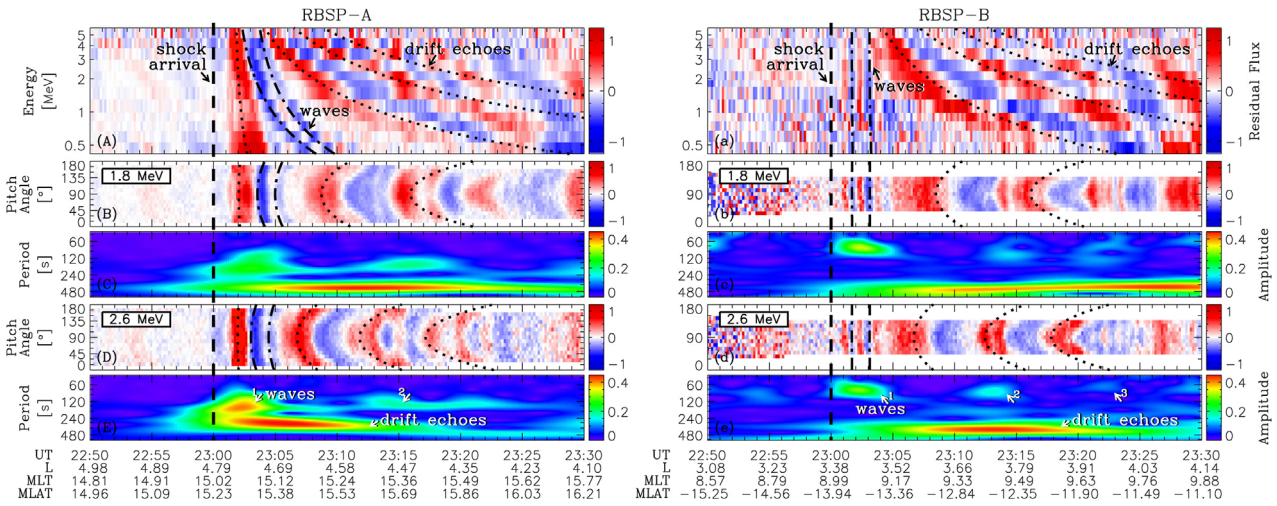

FIGURE 4
Characteristic signatures of radiation belt electrons in the form of wavelet amplitude spectrograms (Panels C, E, c, and e) and residual fluxes (Panels A, B, D, a, b, and d, corresponding to the original electron fluxes in Figures 2A, 2I, 2K, 2a, 2i, 2k).

where B_E is the magnitude of the geomagnetic field in the equatorial plane on the Earth's surface, $R_E \simeq 6.37 \times 10^3\ km$ is the Earth's radius, e and m_e are the charge and the rest mass of an electron, γ is relativistic Lorentz factor, v and α_{eq} are the velocity and the equatorial pitch angle of the electron, and L is the drift shell parameter.

In terms of the one-kick scenario, electrons can be energized as they traverse the IEF. The energization is most efficient when the electron motion matches the pulse propagation. Particularly, in the dusk flank, the azimuthal propagation of the IEF is in the same direction of the electron drift motion, which allows for a longer interaction time between the pulse and the electrons. On the contrary, the interaction time is shorter in the dawn flank, since the azimuthal velocities of the propagating pulse and the drifting electrons are in opposite directions. In other words, electrons in the dusk side may accumulate a larger net energy change. Thus, it is commonly found that the (equivalent) source region of the prompt electron flux variations produced by the shock-induced IEF is located in the dusk-side magnetosphere (Kanekal et al., 2016; Liu et al., 2017; Patel et al., 2019; Liu et al., 2019). Although the electron energy change occurs during the single passage of the IEF, particle detectors may observe a series of subsequent echoes, owing to the periodicity of the drift motion. In this case, the timing of the drift echoes can be theoretically derived by Equations 1, 2, with t^* and ϕ^* assigned as the equivalent time and location at which the electrons are most effectively accelerated by IEF. As shown in Figures 2, 4, the drift echoes observed in the present IPS event are consistent with one-kick scenario. Specifically, an almost dispersionless enhancement of energetic electron flux was first recorded by RBSP-A in the dusk-side outer radiation belt, indicating that the spacecraft was located in the equivalent acceleration region. The subsequent echoes detected by both RBSP-A and RBSP-B exhibited dependence on energy and pitch angle. Moreover, we derive the times t_n at which the drift echoes were expected to be observed in accordance to Equations 1, 2 (with the parameters assigned as $t^* = 23{:}01{:}45\ UT$ and $\phi^* = 14$). The theoretically predicted echoes (denoted by the dotted lines in Figure 4) agree with the actual measurements by the Van Allan Probes. Therefore, we ascribe one of the observed periodic electron flux variations to the drift echoes caused by the shock-induced IEF.

As for the continuous ULF wave-particle interaction, the oscillations of the particle fluxes within the wave active region are independent of pitch angle, thereby appearing as straight vertical stripes in the pitch angle-time spectrogram (Zong et al., 2009; Claudepierre et al., 2013; Chen et al., 2017). In addition, as the particles proceed with their drift motion, the oscillating signatures could also be observed outside the wave active region when the detector encounters those particles that were once modulated by the azimuthally localized ULF wave (Li et al., 2017). Since the drift velocity varies with pitch angle, the modulation patterns (i.e., the straight vertical stripes in the wave active region) would be distorted and transformed into curved boomerang stripes (Hao et al., 2017). Accordingly, the different-shaped stripes are regarded as the diagnostic particle signatures of the localized ULF wave-particle interaction (Zhao et al., 2020). For the present event, the vertical stripes of ~90 s cadence were observed by VAP-B, along with the oscillations of electric and magnetic fields at the same period. Meanwhile, VAP-A, separated by ~6 MLT, detected boomerang stripes with the absence of the corresponding wave electric and magnetic fields. Note that the distortion of the stripes depends on the energy and pitch angle of the electrons and the distance between the wave active region and the detector along the electron drift trajectory. Hence, we can employ Equations 1, 2 to quantitatively examine the correlation between the different-shaped stripes observed severally by the twin Van Allen Probes. Specifically, for each of the stripes, we define t^* and ϕ^* as the time when the straight vertical stripe was observed by RBSP-B and the location of the wave active region (represented by the MLT of RBSP-B), respectively. Then, we can derive the time t at which the

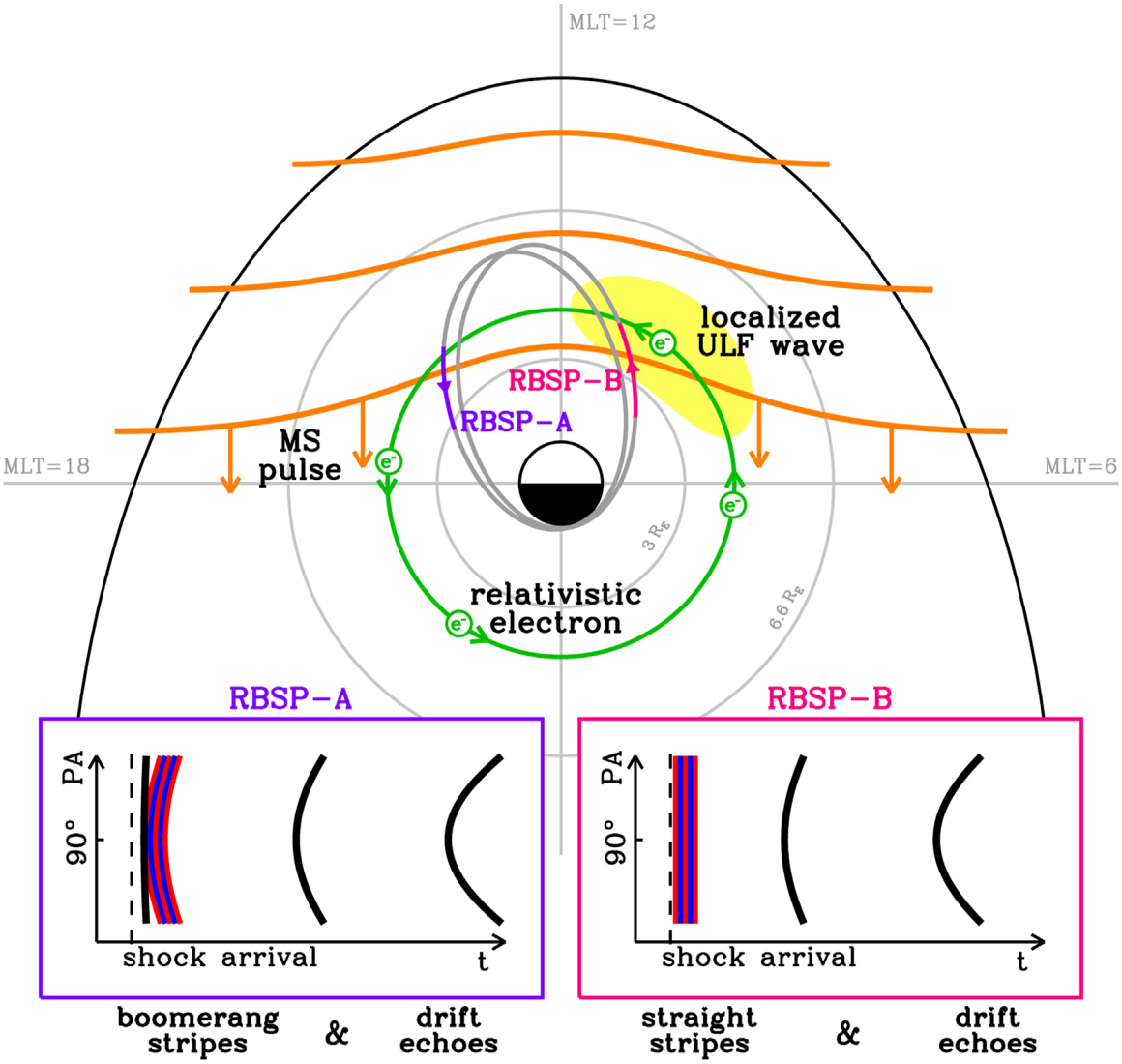

FIGURE 5
Schematic of the shock-induced radiation belt dynamics and the characteristic particle signatures.

other spacecraft would observe the distorted stripe by assigning ϕ as the MLT of RBSP-A and $n = 1$. As presented by the dashed-dotted lines in Figure 4, the shape and timing of the boomerang stripes are well reproduced. Thus, we verify that the other periodic particle signature, namely, the straight and boomerang-shaped stripes at the period of ~90 *s*, is the manifestation of the localized ULF wave-particle interaction.

In addition, we present the wavelet analysis of the 90° fluxes in Figures 4C, E, c, e. On the one hand, the long horizontal patterns in the wavelet amplitude spectrograms refer to the drift echoes. Consistency can be found among the wavelet period corresponding to the horizontal patterns here, the recurrence time of the drift echoes as shown in Figures 2, 4, and the drift period of the electrons as described in 2. On the other hand, 3 isolated amplitude enhancement appeared at ~90 *s*, which agrees with the 3 repeated compression of the magnetosphere observed by THEMIS-E (Figure 1e).

Finally, We sketch the combined effect of the shock-induced IEF and localized ULF waves in Figure 5. On the one hand, the IEF efficiently accelerated the energetic electrons in the dusk-side magnetosphere and caused the prompt electron flux enhancements. The periodic drift motion of the accelerated electrons gave rise to the recurrences of subsequent echoes. On the other hand, the azimuthally localized ULF waves produced the straight and boomerang-shaped stripes in the particle signatures observed inside and outside the wave active region, respectively.

4 Conclusion

The coordinated observations by the Van Allen Probes during the 7 September 2017 event presented the joint effect of the one-kick acceleration and the continuous interaction with the localized ULF waves. For relativistic electrons, the one-kick acceleration

was most effective in the dusk side, while the ULF wave-particle interaction was localized in the dawn-side magnetosphere in the present event. In a broader context, the two types of periodic electron flux variations, namely, the drift echoes and the different-shaped stripes, can be used as the characteristic particle signatures to discriminate between the one-kick acceleration and the localized ULF wave-particle interaction.

Data availability statement

Publicly available datasets were analyzed in this study. This data can be found here: https://cdaweb.gsfc.nasa.gov/pub/data/.

Author contributions

XC: Conceptualization, Visualization, Writing–original draft. XL: Writing–review and editing, Conceptualization. QZ: Conceptualization, Writing–review and editing. HZ: Conceptualization, Writing–review and editing. YL: Conceptualization, Writing–review and editing. XZ: Conceptualization, Writing–review and editing.

Funding

The author(s) declare that financial support was received for the research, authorship, and/or publication of this article. This work was supported by the Science and Technology Development Fund (FDCT) of Macau (grant number: 002/2024/SKL) and NASA contract NAS5-02099.

Acknowledgments

The authors acknowledge NASA's Space Physics Data Facility for providing the data in this study. XC, XL, and HZ would like to thank the space physics and aeronomy research group at UAF for helpful discussions.

Conflict of interest

The authors declare that the research was conducted in the absence of any commercial or financial relationships that could be construed as a potential conflict of interest.

The author(s) declared that they were an editorial board member of Frontiers, at the time of submission. This had no impact on the peer review process and the final decision.

Generative AI statement

The author(s) declare that no Generative AI was used in the creation of this manuscript.

Publisher's note

All claims expressed in this article are solely those of the authors and do not necessarily represent those of their affiliated organizations, or those of the publisher, the editors and the reviewers. Any product that may be evaluated in this article, or claim that may be made by its manufacturer, is not guaranteed or endorsed by the publisher.

Supplementary material

The Supplementary Material for this article can be found online at: https://www.frontiersin.org/articles/10.3389/fspas.2024.1520141/full#supplementary-material

References

Baker, D. N., Kanekal, S. G., Hoxie, V. C., Batiste, S., Bolton, M., Li, X., et al. (2013). The relativistic electron-proton telescope (rept) instrument on board the radiation belt storm probes (rbsp) spacecraft: characterization of earth's radiation belt high-energy particle populations. *Space Sci. Rev.* 179, 337–381. doi:10.1007/s11214-012-9950-9

Blake, J. B., Carranza, P. A., Claudepierre, S. G., Clemmons, J. H., Crain, W. R., Dotan, Y., et al. (2013). The magnetic electron ion spectrometer (mageis) instruments aboard the radiation belt storm probes (rbsp) spacecraft. *Space Sci. Rev.* 179, 383–421. doi:10.1007/s11214-013-9991-8

Blake, J. B., Kolasinski, W. A., Fillius, R. W., and Mullen, E. G. (1992). Injection of electrons and protons with energies of tens of mev into l < 3 on 24 march 1991. *Geophys. Res. Lett.* 19, 821–824. doi:10.1029/92GL00624

Chapman, S., and Ferraro, V. C. A. (1940). The theory of the first phase of a geomagnetic storm. *J. Geophys. Res.* 45, 245–268. doi:10.1029/TE045i003p00245

Chen, X. R., Zong, Q. G., Zhou, X. Z., Blake, J. B., Wygant, J. R., and Kletzing, C. A. (2017). Van Allen Probes observation of a 360° phase shift in the flux modulation of injected electrons by ULF waves. *Geophys. Res. Lett.* 44, 1614–1624. doi:10.1002/2016GL071252

Claudepierre, S. G., Mann, I. R., Takahashi, K., Fennell, J. F., Hudson, M. K., Blake, J. B., et al. (2013). Van allen probes observation of localized drift resonance between poloidal mode ultra-low frequency waves and 60 kev electrons. *Geophys. Res. Lett.* 40, 4491–4497. doi:10.1002/grl.50901

Dessler, A. J., Francis, W. E., and Parker, E. N. (1960). Geomagnetic storm sudden-commencement rise times. *J. Geophys. Res.* 65, 2715–2719. doi:10.1029/jz065i009p02715

Elkington, S. R., Hudson, M. K., Wiltberger, M. J., and Lyon, J. G. (2002). Mhd/particle simulations of radiation belt dynamics. *J. Atmos. Solar-Terrestrial Phys.* 64, 607–615. doi:10.1016/S1364-6826(02)00018-4

Foster, J. C., Wygant, J. R., Hudson, M. K., Boyd, A. J., Baker, D. N., Erickson, P. J., et al. (2015). Shock-induced prompt relativistic electron acceleration in the inner magnetosphere. *J. Geophys. Res. Space Phys.* 120, 1661–1674. doi:10.1002/2014JA020642

Friedel, R. H. W., Reeves, G. D., and Obara, T. (2002). Relativistic electron dynamics in the inner magnetosphere - a review. *J. Atmos. Solar-Terrestrial Phys.* 64, 265–282. doi:10.1016/S1364-6826(01)00088-8

Hamlin, D. A., Karplus, R., Vik, R. C., and Watson, K. M. (1961). Mirror and azimuthal drift frequencies for geomagnetically trapped particles. *J. Geophys. Res.* 66, 1–4. doi:10.1029/JZ066i001p00001

Hao, Y. X., Zong, Q.-G., Wang, Y. F., Zhou, X.-Z., Zhang, H., Fu, S. Y., et al. (2014). Interactions of energetic electrons with ulf waves triggered by interplanetary shock: van allen probes observations in the magnetotail. *J. Geophys. Res. Space Phys.* 119, 8262–8273. doi:10.1002/2014JA020023

Hao, Y. X., Zong, Q.-G., Zhou, X.-Z., Rankin, R., Chen, X. R., Liu, Y., et al. (2017). Relativistic electron dynamics produced by azimuthally localized poloidal mode ulf waves: boomerang-shaped pitch angle evolutions. *Geophys. Res. Lett.* 44, 7618–7627. doi:10.1002/2017GL074006

Hao, Y. X., Zong, Q. G., Zhou, X. Z., Rankin, R., Chen, X. R., Liu, Y., et al. (2019). Global-scale ulf waves associated with ssc accelerate magnetospheric ultrarelativistic electrons. *J. Geophys. Res. Space Phys.* 124, 1525–1538. doi:10.1029/2018JA026134

Hudson, M., Jaynes, A., Kress, B., Li, Z., Patel, M., Shen, X., et al. (2017). Simulated prompt acceleration of multi-mev electrons by the 17 march 2015 interplanetary shock. *Front. Neurosci.* 122, 10036–10046. doi:10.1002/2017JA024445

Hudson, M. K., Elkington, S. R., Li, Z., and Patel, M. (2020). Drift echoes and flux oscillations: a signature of prompt and diffusive changes in the radiation belts. *J. Atmos. Solar-Terrestrial Phys.* 207, 105332. doi:10.1016/j.jastp.2020.105332

Hudson, M. K., Elkington, S. R., Lyon, J. G., Marchenko, V. A., Roth, I., Temerin, M., et al. (1997). Simulations of radiation belt formation during storm sudden commencements. *J. Geophys. Res. Space Phys.* 102, 14087–14102. doi:10.1029/97JA03995

Jacobs, J. A., Kato, Y., Matsushita, S., and Troitskaya, V. A. (1964). Classification of geomagnetic micropulsations. *J. Geophys. Res.* 69, 180–181. doi:10.1029/JZ069i001p00180

Kanekal, S. G., Baker, D. N., Fennell, J. F., Jones, A., Schiller, Q., Richardson, I. G., et al. (2016). Prompt acceleration of magnetospheric electrons to ultrarelativistic energies by the 17 march 2015 interplanetary shock. *J. Geophys. Res. Space Phys.* 121, 7622–7635. doi:10.1002/2016JA022596

Kletzing, C. A., Kurth, W. S., Acuna, M., MacDowall, R. J., Torbert, R. B., Averkamp, T., et al. (2013). The electric and magnetic field instrument suite and integrated science (emfisis) on rbsp. *Space Sci. Rev.* 179, 127–181. doi:10.1007/s11214-013-9993-6

Li, L., Zhou, X.-Z., Zong, Q.-G., Rankin, R., Zou, H., Liu, Y., et al. (2017). Charged particle behavior in localized ultralow frequency waves: theory and observations. *Geophys. Res. Lett.* 44, 5900–5908. doi:10.1002/2017GL073392

Li, X., Roth, I., Temerin, M., Wygant, J. R., Hudson, M. K., and Blake, J. B. (1993). Simulation of the prompt energization and transport of radiation belt particles during the march 24, 1991 ssc. *Geophys. Res. Lett.* 20, 2423–2426. doi:10.1029/93GL02701

Liu, Y., Zong, Q. G., Zhou, X. Z., Hao, Y. X., and Liu, Z. Y. (2019). Understanding electron dropout echoes induced by interplanetary shocks: test particle simulations. *J. Geophys. Res. Space Phys.* 124, 6759–6775. doi:10.1029/2019JA027018

Liu, Z. Y., Zong, Q.-G., Hao, Y. X., Zhou, X.-Z., Ma, X. H., and Liu, Y. (2017). Electron dropout echoes induced by interplanetary shock: a statistical study. *J. Geophys. Res. Space Phys.* 122, 8037–8050. doi:10.1002/2017JA024045

Mann, I. R., Lee, E. A., Claudepierre, S. G., Fennell, J. F., Degeling, A., Rae, I. J., et al. (2013). Discovery of the action of a geophysical synchrotron in the earth's van allen radiation belts. *Nat. Commun.* 4, 2795. doi:10.1038/ncomms3795

Patel, M., Li, Z., Hudson, M., Claudepierre, S., and Wygant, J. (2019). Simulation of prompt acceleration of radiation belt electrons during the 16 july 2017 storm. *Geophys. Res. Lett.* 46, 7222–7229. doi:10.1029/2019GL083257

Ripoll, J. F., Claudepierre, S. G., Ukhorskiy, A. Y., Colpitts, C., Li, X., Fennell, J. F., et al. (2020). Particle dynamics in the earth's radiation belts: review of current research and open questions. *J. Geophys. Res. Space Phys.* 125, 1–48. doi:10.1029/2019JA026735

Schiller, Q., Kanekal, S. G., Jian, L. K., Li, X., Jones, A., Baker, D. N., et al. (2016). Prompt injections of highly relativistic electrons induced by interplanetary shocks: a statistical study of van allen probes observations. *Geophys. Res. Lett.* 43, 12317–12324. doi:10.1002/2016GL071628

Southwood, D. J., and Kivelson, M. G. (1981). Charged particle behavior in low-frequency geomagnetic pulsations 1. transverse waves. *J. Geophys. Res.* 86, 5643–5655. doi:10.1029/JA086iA07p05643

Wilken, B., Goertz, C. K., Baker, D. N., Higbie, P. R., and Fritz, T. A. (1982). The ssc on july 29, 1977 and its propagation within the magnetosphere. *J. Geophys. Res.* 87, 5901–5910. doi:10.1029/ja087ia08p05901

Wygant, J., Mozer, F., Temerin, M., Blake, J., Maynard, N., Singer, H., et al. (1994). Large amplitude electric and magnetic field signatures in the inner magnetosphere during injection of 15 mev electron drift echoes. *Geophys. Res. Lett.* 21, 1739–1742. doi:10.1029/94GL00375

Wygant, J. R., Bonnell, J. W., Goetz, K., Ergun, R. E., Mozer, F. S., Bale, S. D., et al. (2013). The electric field and waves instruments on the radiation belt storm probes mission. *Space Sci. Rev.* 179, 183–220. doi:10.1007/s11214-013-0013-7

Zhang, D., Liu, W., Li, X., Sarris, T. E., Hao, Y., and Zhang, Z. (2024). Surfing acceleration of radiation belt relativistic electrons induced by the propagation of interplanetary shock. *Geophys. Res. Lett.* 51. doi:10.1029/2024GL109285

Zhang, D., Liu, W., Li, X., Sarris, T. E., Wang, Y., Xiao, C., et al. (2020). Relation between shock-related impulse and subsequent ulf wave in the earth's magnetosphere. *Geophys. Res. Lett.* 47. doi:10.1029/2020GL090027

Zhao, X. X., Hao, Y. X., Zong, Q. G., Zhou, X. Z., Yue, C., Chen, X. R., et al. (2020). Origin of electron boomerang stripes: localized ulf wave-particle interactions. *Geophys. Res. Lett.* 47. doi:10.1029/2020GL087960

Zhou, X., Wang, Z., Zong, Q., Rankin, R., Kivelson, M. G., Chen, X., et al. (2016). Charged particle behavior in the growth and damping stages of ultralow frequency waves: theory and van allen probes observations. *J. Geophys. Res. Space Phys.* 121, 3254–3263. doi:10.1002/2016JA022447

Zong, Q.-G., Wang, Y. F., Zhang, H., Fu, S. Y., Zhang, H., Wang, C. R., et al. (2012). Fast acceleration of inner magnetospheric hydrogen and oxygen ions by shock induced ulf waves. *J. Geophys. Res. Space Phys.* 117. doi:10.1029/2012JA018024

Zong, Q. G., Zhou, X. Z., Wang, Y. F., Li, X., Song, P., Baker, D. N., et al. (2009). Energetic electron response to ulf waves induced by interplanetary shocks in the outer radiation belt. *J. Geophys. Res. Space Phys.* 114, 1–11. doi:10.1029/2009JA014393